

$S_1(^1A_1) \leftarrow S_0(^1A_1)$ transition of benzo[*g,h,i*]perylene in supersonic jets and rare gas matrices

G. Rouillé, M. Arold, A. Staicu, S. Krasnokutski, and F. Huisken^{a)}*Institut für Festkörperphysik, Friedrich-Schiller-Universität Jena, Helmholtzweg 3, D-07743 Jena, Germany*

Th. Henning

Max-Planck-Institut für Astronomie, Königstuhl 17, D-69117 Heidelberg, Germany

X. Tan and F. Salama

Space Science Division, National Aeronautics and Space Administration (NASA) Ames Research Center, Mail Stop 245-6, Moffett Field, California 94035-1000

(Received 20 February 2007; accepted 19 March 2007; published online 7 May 2007)

The study of the $S_1(^1A_1) \leftarrow S_0(^1A_1)$ transition of benzo[*g,h,i*]perylene (BghiP, $C_{22}H_{12}$) in supersonic jets and solid rare gas matrices is reported. In the jet-cooled spectrum, the origin band position is located at $25\,027.1 \pm 0.2\text{ cm}^{-1}$, the assignment being supported by the analysis of vibrational shifts and rotational band contours. Except for the origin band, which is weak, all bands are attributed to the fundamental excitation of nontotally symmetric b_1 vibrational modes of S_1 . The intensity pattern is interpreted as a consequence of the weak oscillator strength of the electronic transition combined with intensity-borrowing through vibronic interaction between the $S_1(^1A_1)$ and $S_2(^1B_1)$ states. The spectra of the $S_1(^1A_1) \leftarrow S_0(^1A_1)$ and $S_2(^1B_1) \leftarrow S_0(^1A_1)$ transitions have also been measured for BghiP in solid neon and argon matrices. The comparison of the redshifts determined for either transition reveals that the polarizability of BghiP is larger in its S_2 than in its S_1 state. Bandwidths of 2.7 cm^{-1} measured in supersonic jets, which provide conditions relevant for astrophysics, are similar to those of most diffuse interstellar bands. The electronic transitions of BghiP are found to lie outside the ranges covered by present databases. From the comparison between experimental spectra and theoretical computations, it is concluded that the accuracy of empirical and *ab initio* approaches in predicting electronic energies is still not sufficient to identify astrophysically interesting candidates for spectroscopic laboratory studies. © 2007 American Institute of Physics. [DOI: 10.1063/1.2727467]

I. INTRODUCTION

Polycyclic aromatic hydrocarbons (PAHs) form a family of molecules attracting much attention because of their relation to environmental issues. PAHs, neutral or ionized, are also of great interest to astrophysics. They have been proposed as carriers of the still unassigned diffuse interstellar bands (DIBs).¹ With the aim of contributing to the identification of molecular species present in the interstellar medium, our groups have carried out spectroscopic investigations of neutral²⁻⁵ and cationic⁶⁻⁹ PAHs in supersonic jets.

As PAH samples are solid under normal conditions, studies of isolated molecules are not straightforward, and investigations have proceeded along with the development of spectroscopy techniques. Absorption and emission spectra were first extensively studied for PAHs dispersed in organic solvents, liquid or frozen, and sometimes in the gas phase at relatively high temperatures. The drawback of studies with solvents is the broadening and shifting of spectral features caused by interactions between the species under investigation and the solvent. But an advantage over the early gas phase studies was the possibility to work at low tempera-

tures, which makes spectra somewhat simpler by eliminating the contribution of thermally populated states and by suppressing the homogeneous broadening according to the Shpolskii effect.¹⁰ The use of argon and then neon as host media for matrix isolation spectroscopy was another improvement given the weaker interaction between the solute and the rare gas atoms. More recently, the host medium underwent another evolution with the use of liquid helium droplets.¹¹

In the meantime, gas phase techniques made their own progress. Heated pulsed nozzles make it possible to increase the vapor pressure of a normally solid species and to cool the molecules to temperatures below 50 K by expanding the vapor with a carrier gas through a nozzle into vacuum. Sensitive spectroscopy techniques such as laser-induced fluorescence spectroscopy and cavity ring-down laser absorption spectroscopy (CRLAS) can then be applied to probe the species at low temperature under collision-free conditions, which are relevant for astrophysics.

The absorption and emission spectra of the most common PAHs have been studied with some of the techniques just mentioned. This includes benzo[*g,h,i*]perylene (BghiP, $C_{22}H_{12}$), also known as 1,12-benzoperylene or 1,12-benzperylene. The absorption spectrum of BghiP has been

^{a)}Also at Max-Planck-Institut für Astronomie, Königstuhl 17, D-69117 Heidelberg, Germany. Electronic mail: friedrich.huisken@uni-jena.de

studied in the gas phase at elevated temperature,¹² in organic solvents,^{12–20} and in neon matrix.²¹ As indirect absorption measurements, excitation spectra have been reported for the hot gas phase.²² Finally, a high resolution absorption spectrum recorded at 5 K in *n*-octane has been published in the spectral atlas of Nakhimovsky *et al.*²³

Absorption spectra of benzo[*g,h,i*]perylene in the hot gas phase and in liquid or frozen solutions showing both the $S_1 \leftarrow S_0$ and $S_2 \leftarrow S_0$ transitions have been reported.^{12,13,16,19,20} They reveal that the strength of $S_1 \leftarrow S_0$ is much weaker than that of $S_2 \leftarrow S_0$. Moreover, Langelaar *et al.*¹⁶ have demonstrated experimentally that the S_1 and S_2 states of BghiP, which possesses the symmetry elements of point group C_{2v} , transform according to the 1A_1 and 1B_1 irreducible representations, respectively. As a convention, the x axis is set in the present work parallel to the long axis of the molecule and the y axis perpendicular to the molecular plane. As a consequence, when citing publications where the Mulliken convention²⁴ has been used, the notation of irreducible representations has been corrected, i.e., B_1 and B_2 have been interchanged.

With BghiP in liquid or frozen solutions, authors have determined the origin of the $S_1 \leftarrow S_0$ transition to be in the 24 550–24 675 cm^{-1} range,^{14,19,20,25} while the $S_2 \leftarrow S_0$ (0-0) transition was located between 25 840–26 062 cm^{-1} .^{14,19} An energy separation of $\sim 1350 \text{ cm}^{-1}$ between S_1 and S_2 can be derived for BghiP in these solutions. For comparison, an attempt to estimate this energy separation in the unperturbed molecule was made by Aihara *et al.*¹² Using a simple model for solvent effects, they predicted an energy difference of 2000 cm^{-1} between S_1 and S_2 , which is larger than the separation observed in solution.

Recently, Tan and Salama⁵ studied the $S_2 \leftarrow S_0$ system of BghiP by CRLAS in a supersonic jet. They observed an intermediate level structure due to vibronic interaction between the S_1 and S_2 states. Although the investigated range did not include the region of the $S_1 \leftarrow S_0$ origin, they predicted its position at 25 795 cm^{-1} (in vacuum). This was achieved by fitting a calculated spectrum to the observed intermediate level structure and taking into account the vibronic interaction between S_1 and S_2 .⁵

Most interestingly, four bands of benzo[*g,h,i*]perylene lying in an energy range lower than that scanned by Tan and Salama have been pointed out by Bermudez and Chan²⁶ in the jet-cooled excitation spectrum of coronene contaminated by BghiP. We have evaluated the position of the lowest BghiP band to be at 25 795 cm^{-1} in air, that is, 25 788 cm^{-1} in vacuum, which would be in excellent agreement with the position of the $S_1 \leftarrow S_0$ origin band predicted by Tan and Salama.⁵ On the other hand, since Tan and Salama determined the origin of the $S_2 \leftarrow S_0$ transition at 27 132 cm^{-1} , by taking into account the energy separation of 2000 cm^{-1} estimated by Aihara *et al.*,¹² one expects to find the origin of the $S_1 \leftarrow S_0$ transition near 25 100 cm^{-1} . Moreover, making use of solvatochromism in *n*-alkanes, Renge²⁷ has extrapolated a value of $24\,994 \pm 20 \text{ cm}^{-1}$ for the origin of $S_1 \leftarrow S_0$. As a consequence, it appears unlikely that the origin position predicted by Tan and Salama is correct or that the lowest energy band observed by Bermudez and Chan is the 0_0^0 band.

Support to locate precisely the $S_1 \leftarrow S_0$ origin band is not provided by theoretical calculations. Early calculations of electronic transition energies and oscillator strengths were published by Hummel and Ruedenberg²⁸ and later by Marañon *et al.*²⁹ Either work made use of semiempirical models, the former yielding different symmetries for 1A_1 and 1B_1 for S_1 , depending on which approximations were made, the latter yielding 1B_1 . More recently, calculations were performed with a method based on the time-dependent density-functional response theory (TD-DFT). This method also yielded 1B_1 instead of 1A_1 as the symmetry of the S_1 state and as a consequence a rather strong oscillator strength for the $S_1 \leftarrow S_0$ transition.²¹ On the other hand, Palewska and Chojnacki³⁰ calculated the electronic transition energies and oscillator strengths with the Zerner intermediate neglect of diatomic differential overlap (ZINDO) semiempirical approach.³¹ Their results, including the symmetries of the electronic states, compare favorably with the observed spectra. Lastly, Tan and Salama⁵ carried out new calculations, again based on TD-DFT, but with a new approach that proved to be more effective than that used by Chillier *et al.*²¹ since the S_1 state was found to be of the 1A_1 species.

The present work aims at improving our knowledge of the $S_1({}^1A_1) \leftarrow S_0({}^1A_1)$ transition of benzo[*g,h,i*]perylene by introducing new experimental results. These are principally the unperturbed origin band position of the transition, which we expect to find near 25 000 cm^{-1} , and the fundamental vibrational frequencies in the S_1 state. These data are essential for comparison with astronomical observations.

II. EXPERIMENT

A. Cavity ring-down laser absorption spectroscopy in supersonic jets

The cavity ring-down laser absorption spectrometer has been described previously,^{2,3} but some of its components have been renewed. The laser source is a tunable dye laser (Continuum ND6000) pumped by a pulsed Nd:YAG (YAG denotes yttrium aluminum garnet) laser (Continuum Surelite II-20) with a pulse duration of 5 ns. The dye laser oscillator was equipped with a single grating of 1800 l/mm yielding a specified linewidth of 0.10 cm^{-1} at 750 nm. As dye we used LDS765 (Radiant Dyes Chemie) dissolved in methanol, which allowed us to cover the entire range of interest for this study.

The visible beam emitted by the dye laser was frequency-doubled by means of a potassium dideuterium phosphate KD^*P crystal (Continuum DCC1), the orientation of which was optimized by a tracking system. Without focusing, the resulting ultraviolet beam was directed onto a pinhole (diameter of 57 μm) and collimated by a converging fused-silica lens ($f=100 \text{ mm}$). After having blocked the rings surrounding the Airy spot with an iris, the ultraviolet beam was injected into the 1-m-long cavity formed by a pair of identical high-reflectance mirrors with a radius of curvature of 6 m (Los Gatos Research). A reflectance of at least 0.999 89 at 399.8 nm was determined by measuring the decay time when the molecular beam chamber was evacuated. In order to block the stray light at the visible fundamental

wavelength emitted by the dye laser, the photomultiplier module detector (Hamamatsu H6780-02) placed behind the exit mirror was protected by a color filter (Schott BG39).

The laser linewidth before frequency doubling was estimated to be 0.22 cm^{-1} at 784.2 nm by fitting a Lorentzian to the profile of a Ne I absorption line observed in a hollow cathode lamp (Hamamatsu L233-26NU) via the optogalvanic effect. This value is approximately twice as large as the specified linewidth. From the measured line profile, the linewidth after doubling was estimated to be 0.20 cm^{-1} . Several Ne I lines were used as reference³² for an absolute calibration of the laser wavelength. The resulting uncertainty of the wave number scale is 0.04 cm^{-1} relative to the Ne I line positions. All wave numbers and wavelengths reported for the present CRLAS measurements are given for vacuum unless otherwise noted.

The jet source, a heated pulsed valve, has also been described previously.³ It consists of a commercial solenoid valve (General Valve Series 9) to which a small chamber containing the sample has been attached. This sample chamber can be heated up to $500\text{ }^{\circ}\text{C}$ with a stability of $1\text{ }^{\circ}\text{C}$. For the present study, argon (Linde, purity of 5.0) was used as carrier gas. The benzo[*g,h,i*]perylene sample was provided by Fluka (purity $\geq 98\%$). The valve was operated with a repetition rate of 20 Hz, the open position being maintained for $600\text{ }\mu\text{s}$. As stagnation pressure, we employed 1.5 bar, yielding a background pressure of 1.35×10^{-2} mbar in the expansion chamber. The gas jet was probed 3 mm downstream from the nozzle exit.

A master program written in LABVIEW language executes the data acquisition and controls the wavelength position of the dye laser through its legacy control program. In every spectrum acquired for this study, a data point represents an average over 64 laser shots. The present spectra were established by subtracting a background signal from the raw data. We associate this background with the reflectance curve of the cavity mirrors and the scattering losses caused by the gas jet. In some close-up spectra for which it will be indicated, we have also subtracted an interference signal that built up in the exit mirror of the cavity.³³ The subtracted interference pattern was calculated with an Airy function based on the mirror parameters which are the thickness and index of refraction of the substrate as well as the reflectance at each face.

B. Absorption spectrum in neon matrix

Ne-matrix experiments were performed at NASA Ames. The experimental apparatus has been described elsewhere²¹ and only a synopsis is given here. Briefly, the experimental apparatus consists of a cryogenic sample chamber that is part of a high-vacuum system and consists of four ports at 90° and two gas injection inlets at 45° . The sample holder suspended at the center of the chamber is cooled down to 4.2 K by a liquid He transfer cryostat (Hansen Associates HLT-183). The substrate (sapphire) can be positioned to face alternatively the spectroscopy ports, the gas injection inlets, an irradiation lamp, or vacuum deposition furnace. A deuterium lamp (Hamamatsu L1626) provides spectral output from

160 to 360 nm, and a quartz tungsten halogen lamp (Ushio FCR) provides output from 320 to 2500 nm. Spectra of isolated BghiP were recorded from 180 to 1000 nm with a nominal resolution of 0.1 nm using a 0.5 m, triple grating monochromator (Acton Research Corporation) and a charge coupled device camera array (Princeton Instruments) mounted on the exit port and interfaced to a computer system. Benzo[*g,h,i*]perylene (Aldrich, 98%) was purified through a series of evaporation procedures. Neon (Cryogenic Rare Gas, 99.9995%) was used without further purification. The vaporization of BghiP was performed using a resistively heated Pyrex tube, which was mounted on the sample chamber and positioned between 2 and 3 cm from the cold sapphire window. The temperature of the tube was monitored using a chromel/alumel thermocouple mounted on the exterior of the tube. Benzo[*g,h,i*]perylene was heated to about $150\text{ }^{\circ}\text{C}$ before the substrate window was turned towards the sample. The operating heating temperature was set at $155\text{ }^{\circ}\text{C}$. The PAH sample was simultaneously condensed with the neon gas onto the cold substrate. The matrix-gas flow rate was set at 12 mmol/h for neon to reduce the light scattering of the matrix. Based on these parameters, the Ne/BghiP ratio is estimated to be in excess of 1000/1.

C. Absorption spectrum in argon matrix

The argon matrix was grown onto a CaF_2 substrate placed inside a flow cell that was evacuated by a turbomolecular pump backed by a mechanical pump. Under vacuum, the substrate was cooled down to 12 K by a He closed-cycle cryostat (APD Cryogenics Inc.), its temperature being monitored and stabilized by a sensor and controller system (Lake-Shore). When the temperature reached 12 K, the matrix deposition was initiated by establishing an argon (Linde, purity of 5.6) flow maintained at 3.7 SCCM (SCCM denotes cubic centimeter per minute at STP), yielding a static pressure of 3×10^{-4} mbar in the cell. During the growth of the matrix, the BghiP sample was kept at $150\text{ }^{\circ}\text{C}$ in an oven made from a copper tube on which a heating element was mounted. After 90 min, the growth process was stopped and the heating element was removed from the oven. A pair of optical fibers connected the flow cell to the spectrometer (Perkin Elmer Lambda 19). For the present study, the scanning speed was set to 30 nm/min, and the slit was selected to obtain a resolution of 0.48 nm at $\lambda=400\text{ nm}$. The spectrometer featured an internal wavelength calibration system that yielded an accuracy of 0.15 nm, corresponding to 9.4 cm^{-1} at 400 nm. In order to increase the signal-to-noise ratio, the spectrum was scanned 100 times. A value of 1.000 279 was used for the refractive index of air to convert the measured wavelengths to vacuum wave numbers.

III. RESULTS

A. Cavity ring-down laser absorption spectroscopy in supersonic jets

With the bands reported by Bermudez and Chan²⁶ and the predicted positions for the $S_1 \leftarrow S_0$ origin^{12,27} as starting

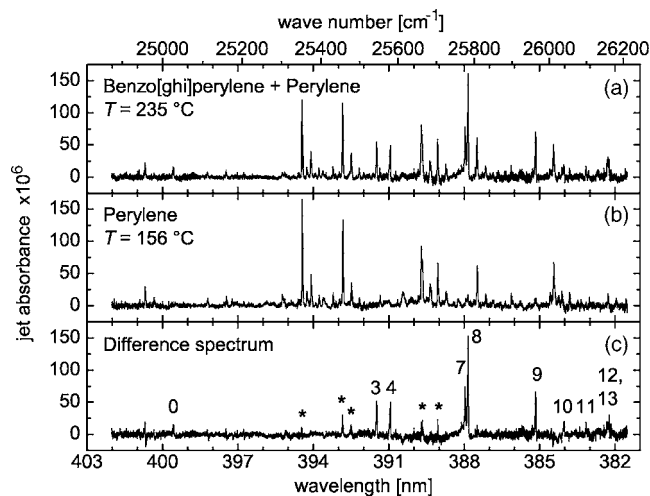


FIG. 1. (a) The $S_1(^1A_1) \leftarrow S_0(^1A_1)$ absorption spectrum of jet-cooled benzo[*g,h,i*]perylene containing traces of perylene. (b) Absorption spectrum of jet-cooled perylene measured for comparison. (c) Difference spectrum highlighting the bands related to BghiP which are labeled with numbers. Features marked with asterisks are residuals from perylene bands and should not be confused with bands of BghiP. The strongest bands related to perylene complexes with argon cause noticeable negative features. Wavelengths are given for vacuum.

points, absorption spectroscopy was carried out over the wavelength range from 380 to 402 nm (24 875–26 320 cm^{-1}).

Figure 1(a) shows an overall spectrum that was obtained by scanning several wavelength ranges in succession. The benzo[*g,h,i*]perylene sample was placed into the source as received and heated up to 235 °C. Numerous bands can be observed which could be separated into two groups according to the behavior of their intensities. As a matter of fact, the absolute intensities of some bands were reproducible from one measurement to the other, whereas those of the other bands depended on the sample used. In particular, the bands for which the intensity varied were not observed in earlier measurements that were carried out with samples labeled with a different lot number. These bands formed a typical pattern recently observed by Tan and Salama,⁴ suggesting that they were due to perylene. Indeed, using high pressure liquid chromatography (HPLC) to analyze the material remaining after an experiment on BghiP during which perylene bands were observed, we could confirm the presence of perylene. But even though the perylene bands had an intensity comparable to the strongest BghiP bands, which could suggest the transformation of BghiP into perylene upon heating, it was found that the molar concentration of perylene in the sample was only of the order of 1%, in agreement with the specifications of the manufacturer.

So as to definitely verify our conjecture, we measured an absorption spectrum for pure perylene (Aldrich, 99+%) under the same conditions, with the exception of the source temperature which was reduced to 156 °C. This spectrum is displayed in Fig. 1(b). The intensities of the perylene bands observed under these conditions were of the same magnitude as those observed with the BghiP sample heated to 235 °C [Fig. 1(a)]. Bands associated with the perylene-Ar and perylene-Ar₂ van der Waals complexes are also present in

TABLE I. Observed positions and vibrational shifts, along with mode assignments, for the bands in the $S_1(^1A_1) \leftarrow S_0(^1A_1)$ transition of jet-cooled benzo[*g,h,i*]perylene. Values in parentheses refer to tentative assignments.

Band position (cm^{-1})	Accuracy (cm^{-1})	Vibrational shift (cm^{-1})	Assignment	Calculated ^a (cm^{-1})
25 027.1	0.2	0	origin	
(25 386.0)	(0.3)	(358.9)	($1b_1$) ₀ ¹	352.5
(25 405.3)	(0.3)	(378.2)	($2b_1$) ₀ ¹	392.0
25 544.6	0.2	517.5	($3b_1$) ₀ ¹	509.1
25 579.8	0.2	552.7	($4b_1$) ₀ ¹	533.2
			($5b_1$) ₀ ¹	600.1
			($6b_1$) ₀ ¹	660.5
25 776.8	0.2	749.7	($7b_1$) ₀ ¹	749.9
25 784.2	0.2	757.1	($8b_1$) ₀ ¹	789.3
25 964.2	0.2	937.1	($9b_1$) ₀ ¹	908.2
26 039.9	0.2	1012.8	($10b_1$) ₀ ¹	1010.6
26 099.1	0.4	1072.0	($11b_1$) ₀ ¹	1067.0
			($12b_1$) ₀ ¹	1101.7
26 158.8	0.3	1131.7	($13b_1$) ₀ ¹	1117.5
			($14b_1$) ₀ ¹	1173.2
26 232.2	0.2	1205.1	($15b_1$) ₀ ¹	1201.4
			($16b_1$) ₀ ¹	1204.4

^aReference 5.

this spectrum, their identification being based on the work of Leutwyler.³⁴ These bands are weaker in Fig. 1(a), a fact that we attribute to the higher temperature of the source in that case.

To reveal the absorption spectrum of benzo[*g,h,i*]perylene, we took the difference between the traces shown in Figs. 1(a) and 1(b) and plotted the result in Fig. 1(c). For a better result, the absorbance in the perylene spectrum was divided by a factor of 1.3. Features labeled with numbers indicate bands of BghiP, with band 0 marking the origin of the $S_1 \leftarrow S_0$ transition. The others correspond to the fundamental excitation of nontotally symmetric b_1 modes to which the numbers refer. For instance, 3 refers to band ($3b_1$)₀¹. We associate one of the features with two bands, ($12b_1$)₀¹ and ($13b_1$)₀¹, because it is significantly broader than the others. Band positions, corresponding vibrational shifts, and detailed assignments are presented in Table I. The arguments leading to these assignments are given in the next paragraphs. Tables reporting the positions, assignments, and vibrational shifts of bands due to perylene and its complexes with one and two argon atoms are available as supplemental material.³⁵

The region of the origin band of $S_1 \leftarrow S_0$ is shown in greater detail in Fig. 2(a). In the upper trace that was recorded with the BghiP sample, the interference background signal previously mentioned has been subtracted and the signal-to-noise ratio has been improved by averaging the data by pairs. The BghiP sample used at that time contained almost no perylene as can be concluded from a comparison with Fig. 1(a). Except for the sample lot number, these measurements were obtained under the same experimental conditions. The lower trace in Fig. 2(a) is a close-up of the perylene spectrum shown in Fig. 1(b). It has been normalized so that its features exhibit the same magnitude as in the up-

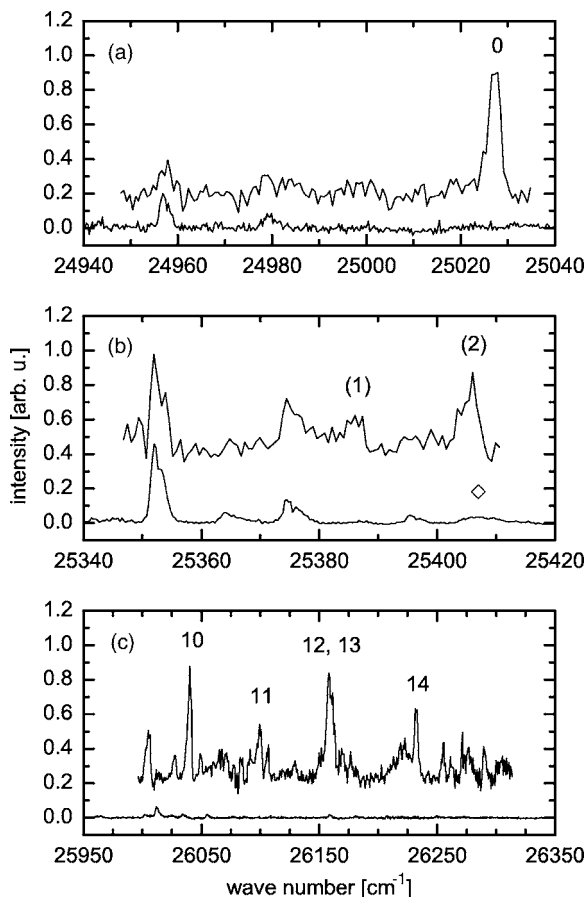


FIG. 2. Comparison in different energy ranges of the $S_1(^1A_1) \leftarrow S_0(^1A_1)$ absorption spectrum of jet-cooled BghiP (upper traces) with the absorption spectrum of jet-cooled perylene (lower traces): (a) The origin band of the $S_1 \leftarrow S_0$ transition of BghiP is indicated with 0. A weak feature at $24\,957.0\text{ cm}^{-1}$ can be associated with a perylene band, showing that the BghiP sample is slightly contaminated. (b) Features marked (1) and (2) are tentatively attributed to bands $(1b_1)_0^1$ and $(2b_1)_0^1$, respectively, in the $S_1 \leftarrow S_0$ transition of BghiP. A band due to the perylene-Ar complex is marked by a diamond (\diamond). (c) Three features labeled by 10, 11, and 14 are attributed to bands $(10b_1)_0^1$, $(11b_1)_0^1$ and $(14b_1)_0^1$ respectively, in the $S_1 \leftarrow S_0$ transition of BghiP. The feature indicated with numbers 12 and 13 is attributed to the close-lying bands $(12b_1)_0^1$ and $(13b_1)_0^1$.

per trace. The comparison of the two traces reveals that the band at $25\,027.1\text{ cm}^{-1}$ corresponds to the transition with the lowest energy that can be attributed to BghiP. This is the *first* reason why we think that this is the origin of the $S_1 \leftarrow S_0$ transition of BghiP.

Figure 2(b) shows the spectral range in which bands corresponding to the fundamental excitation of modes $1b_1$ and $2b_1$ are expected. The lower trace is extracted from the perylene spectrum of Fig. 1(b) and includes five bands that we attribute to the monomer and another one, marked with \diamond , which is due to the complex of perylene with argon. The upper trace has been recorded with a BghiP sample with low perylene content, heated to $251\text{ }^\circ\text{C}$. The main difference to the perylene trace are the two features that are labeled by (1) and (2). The parentheses mean that the identification with bands $(1b_1)_0^1$ and $(2b_1)_0^1$ is tentative. The positions of features (1) and (2) coincide with those of a band of perylene at $25\,386.9\text{ cm}^{-1}$, $(1a_u)_1^1X$, and of the band of the complex, respectively. Here X denotes a transition involving one or sev-

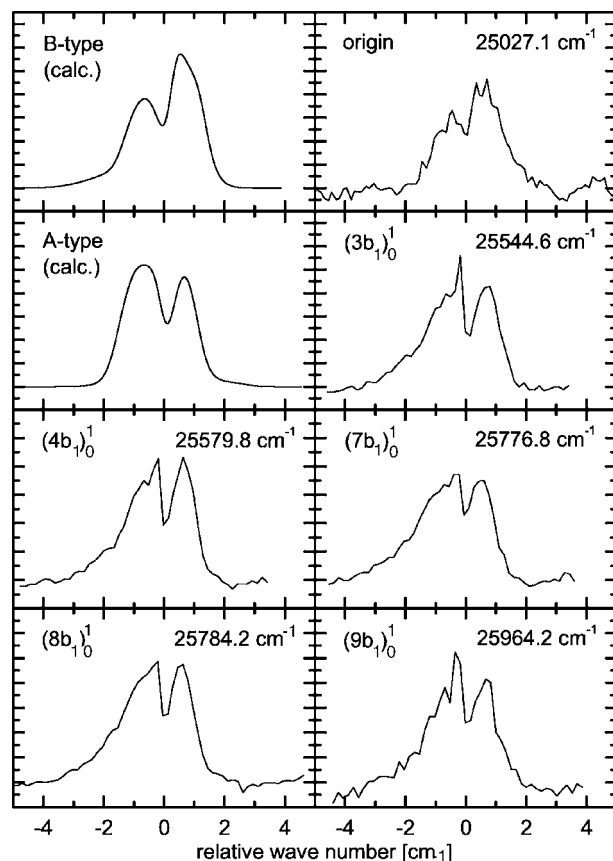


FIG. 3. Calculated A- and B-type rotational band profiles compared with observed band contours. The origin band shows a B-type profile whereas the other bands exhibit an A-type profile.

eral modes we have not determined. The intensities of features (1) and (2), at that higher source temperature, relative to those of the perylene bands, indicate that they are not the bands observed at the same positions in the perylene spectrum. Indeed, feature (1) is stronger than the perylene band X at $25\,364.4\text{ cm}^{-1}$ which is too weak to be clearly seen, whereas band $(1a_u)_1^1X$ should be weaker than X , even under higher temperature conditions. Regarding feature (2), it is as strong as the perylene band $(8a_g)_0^1$ at $25\,352.4\text{ cm}^{-1}$, whereas the increased temperature would weaken any band related to complexes with argon.

The higher energy range, where we have identified four weak bands that we attribute to benzo[*g,h,i*]perylene, is covered by Fig. 2(c). As previously stated, one of the features, labeled by 12 and 13, is significantly broader than its neighbors, its full width at half maximum being 5.9 cm^{-1} compared to 2.7 cm^{-1} for the others. This feature consists either of one band which is broadened by a perturbation, or of two overlapping bands. The latter alternative seems more likely to us. Finally, the next feature is logically assigned to band $(14b_1)_0^1$.

In order to strengthen our assignment, as shown in Fig. 3, rotational contours have been determined for the most intense bands of BghiP. In each case, the background interference signal has been subtracted, with the exception of band $(9b_1)_0^1$ at $25\,964.2\text{ cm}^{-1}$ for which we found it unnecessary. Improvement of the signal-to-noise ratio has been achieved in the origin band spectrum by averaging the data

by pairs. The resulting wavelength step is 0.002 nm, while it is 0.0025 nm for all other bands. On the other hand, for each band from $(3b_1)_0^1$ to $(8b_1)_0^1$, the contour is an average over two spectra recorded under the same conditions. Therefore, in those cases, one point represents an average over 128 laser shots.

In each case, the rotational band contour displays two maxima. But the contour of the band at $25\,027.1\text{ cm}^{-1}$, which is our candidate for the origin band, is different from the others. The two maxima have different heights, the peak on the low-energy side being clearly smaller than the other. For the other bands, the maxima have comparable heights. Moreover, the band at $25\,027.1\text{ cm}^{-1}$ is slightly broadened on the high-energy side whereas the other bands are broadened on the low-energy side.

Together with the measured bands, Fig. 3 shows two calculated contours. The rotational constants for the equilibrium structures of the S_0 and S_1 states were determined by DFT and TD-DFT calculations, respectively.⁵ They are for the electronic ground state $A''=0.014\,704\,8\text{ cm}^{-1}$, $B''=0.010\,922\,1\text{ cm}^{-1}$, and $C''=0.006\,267\,15\text{ cm}^{-1}$. For the excited state we have $A'=0.014\,516\,3\text{ cm}^{-1}$, $B'=0.010\,995\text{ cm}^{-1}$, and $C'=0.006\,256\,33\text{ cm}^{-1}$. The statistical weights of the rotational states in S_0 are 2080 for the states of A_1 and A_2 symmetries and 2016 for the states of B_1 and B_2 symmetries. Therefore, they could be neglected in the simulation of the rotational contours that were calculated with the SPECVIEW program of Stakhursky and Miller.³⁶ Rotational contours of both A and B types have been simulated taking into account rotational quantum numbers up to $J=101$. The rotational lines were given a Lorentzian profile with a width of 0.3 cm^{-1} , and the rotational temperature was set to 40 K to obtain band contours similar to those observed. Since the laser linewidth has been estimated to be 0.2 cm^{-1} , the intrinsic width of a rotational line would be about 0.1 cm^{-1} .

We note that the band observed at $25\,027.1\text{ cm}^{-1}$ has a contour similar to the calculated B -type contour, whereas the other bands exhibit an A -type profile. In the latter case, it should be kept in mind that the influence of excited vibrations is not taken into account in the calculation, explaining differences between observed and calculated contours. Since the S_0 and S_1 states are both of the 1A_1 symmetry species, a B -type profile is expected for the origin band of the $S_1\leftarrow S_0$ transition. Therefore, the contour analysis supports the claim that the band at $25\,027.1\text{ cm}^{-1}$ is the vibrationless origin band. This is the *second* reason for this assignment. The other bands correspond to the excitation of b_1 vibrational modes.

For each band of BghiP for which two maxima can be observed in the rotational contour, the position of the lowest point in the dip that separates the maxima is taken as the band position. It is given with an accuracy of $\pm 1/2$ step to which is added the uncertainty of the wavelength calibration procedure. This concerns only the bands described in Fig. 3. For the other bands, the positions have been estimated by fitting a Lorentzian profile to the observed feature and taking the peak position. Assignments are assisted by comparing the observed vibrational shifts with theoretical vibrational frequencies determined by DFT-based calculations.⁵ Concern-

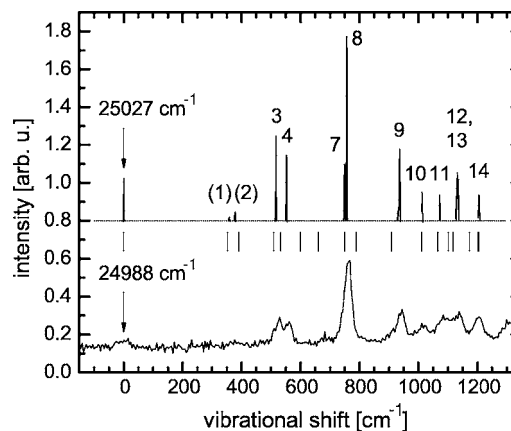


FIG. 4. Comparison of the $S_1({}^1A_1)\leftarrow S_0({}^1A_1)$ absorption spectra of BghiP observed in a supersonic expansion (top) and in a neon matrix (bottom). For the supersonic jet spectrum, only the bands marked in Fig. 1 were plotted. Arrows mark the origin band positions and reveal a redshift of 39 cm^{-1} for the matrix spectrum. Vertical bars indicate the calculated harmonic frequencies for modes $1b_1$ – $16b_1$ relative to the origin (Ref. 5).

ing bands for which an A -type contour has been clearly verified, their assignment to transitions $(3b_1)_0^1$, $(4b_1)_0^1$, $(7b_1)_0^1$, $(8b_1)_0^1$, and $(9b_1)_0^1$ is certain. On the contrary, the association of the two features discussed in Fig. 2(b) with bands $(1b_1)_0^1$ and $(2b_1)_0^1$ is tentative because the band profiles could not be measured with enough details and, according to calculations,⁵ the $(2a_1)_0^1$ band is expected very close to the position of feature (2). Thus, within the spectral range between features (2) and 10, all observed bands are unambiguously caused by the excitation of b_1 modes. This means that the bands $(3a_1)_0^1$ to $(9a_1)_0^1$ which would appear in this spectral range are definitely not observed. As a consequence, it is reasonable to assume that bands involving a_1 modes are not observed at all in the present study. Accordingly, the assignment of bands $(10b_1)_0^1$ – $(14b_1)_0^1$ is made in the order of increasing energy, bands $(12b_1)_0^1$ and $(13b_1)_0^1$ being associated with a single broad feature. We have attributed the higher energy band to $(14b_1)_0^1$ even though the corresponding vibrational shift is closer to the calculated frequencies for $15b_1$ and $16b_1$. An attempt to observe bands $(5b_1)_0^1$ and $(6b_1)_0^1$ was not successful. The correlation between the observed vibrational shifts and theoretical vibrational frequencies which are included in Fig. 4 is fairly good, supporting our assignment.

B. Absorption spectrum in neon matrix

A new absorption spectrum covering the region of the $S_1({}^1A_1)\leftarrow S_0({}^1A_1)$ transition of benzo[*g,h,i*]perylene in a neon matrix is shown in Fig. 4. In contrast to the earlier experiment of Chillier *et al.*,²¹ the signal-to-noise ratio is significantly improved. The comparison between this new spectrum and the absorption spectrum of perylene embedded in a neon matrix³⁷ proves the absence of perylene bands. More specifically, perylene would show prominent bands at 392.4, 395.6, and 397.2 nm.³⁷ These bands are absent in the present spectrum of BghiP in solid neon. The lowest energy band which is observed at $24\,988.3\text{ cm}^{-1}$ is identified as the origin of the $S_1\leftarrow S_0$ transition of BghiP, yielding a redshift of 39 cm^{-1} relative to its position in the jet-cooled spectrum.

TABLE II. Observed positions and vibrational shifts, along with mode assignments, for the bands in the $S_1(^1A_1) \leftarrow S_0(^1A_1)$ transition of benzo[*g,h,i*]perylene in a neon matrix at 4.2 K.

Band position (cm ⁻¹)	Width (cm ⁻¹)	Vibrational shift (cm ⁻¹)	Assignment
24 988.3	50.5	0	origin
25 514.8	32.9	526.5	(3 <i>b</i> ₁) ₀ ¹
25 549.9	21.9	561.6	(4 <i>b</i> ₁) ₀ ¹
25 749.7	28.0	761.4	{ (7 <i>b</i> ₁) ₀ ¹ (8 <i>b</i> ₁) ₀ ¹
25 929.1	31.5	940.8	(9 <i>b</i> ₁) ₀ ¹
26 003.4	29.2	1015.1	(10 <i>b</i> ₁) ₀ ¹
26 078.1	63.8	1089.8	(11 <i>b</i> ₁) ₀ ¹
26 126.4	29.0	1138.1	{ (12 <i>b</i> ₁) ₀ ¹ (13 <i>b</i> ₁) ₀ ¹
26 193.1	34.0	1204.8	(14 <i>b</i> ₁) ₀ ¹

The band pattern for the vibrational excitations below 1250 cm⁻¹ is the same as observed in the supersonic expansion, supporting our previous analysis. Therefore, like in the jet-cooled spectrum, the observed bands relate to excited *b*₁ modes and the excitation of totally symmetric *a*₁ modes is not observed. The band positions, widths, and vibrational shifts observed in the matrix are given in Table II.

As can be seen in Fig. 5, which shows an extended spectrum of BghiP in solid neon, several other features related to the $S_1 \leftarrow S_0$ transition appear at energies higher than 26 250 cm⁻¹. At still higher energies, above 26 700 cm⁻¹, the absorbance increases sharply to reach a maximum at 26 909 cm⁻¹, marking the approximate position of the origin of the $S_2(^1B_1) \leftarrow S_0(^1A_1)$ transition. From this observation, it is concluded that the energy separation between states S_1 and S_2 is smaller in the neon matrix than in the supersonic expansion, the respective values being 1921 and 2105 cm⁻¹. Moreover, the features observed in the neon matrix are one order of magnitude broader than those observed in the gas jet. Both phenomena are consequences of the interaction between the molecule and the rare gas matrix.

C. Absorption spectrum in argon matrix

As seen in Fig. 5, the absorption spectrum of BghiP in solid argon at 12 K between 24 380 and 27 770 cm⁻¹ (360 and 410 nm) shows a series of weak features between 25 000 and 26 000 cm⁻¹ and a much more intense peak at 26 413 ± 11 cm⁻¹ (378.5 nm in air) with a shoulder on the high-energy side. Comparison of our data with literature spectra recorded in organic solvents reveals that the peak at 26 413 cm⁻¹ correlates with the $S_2 \leftarrow S_0$ (0-0) transition of benzo[*g,h,i*]perylene. As a difference to the corresponding feature observed in the neon matrix, it is noticed that, in the argon matrix, the peak is broader and further shifted to lower energies.

The question arises whether some of the weak bands observed in the Ar matrix spectrum between 25 000 and 26 000 cm⁻¹ are due to traces of perylene contained in the BghiP sample. The sample used in this experiment was from the lots that showed a lower concentration of perylene in the

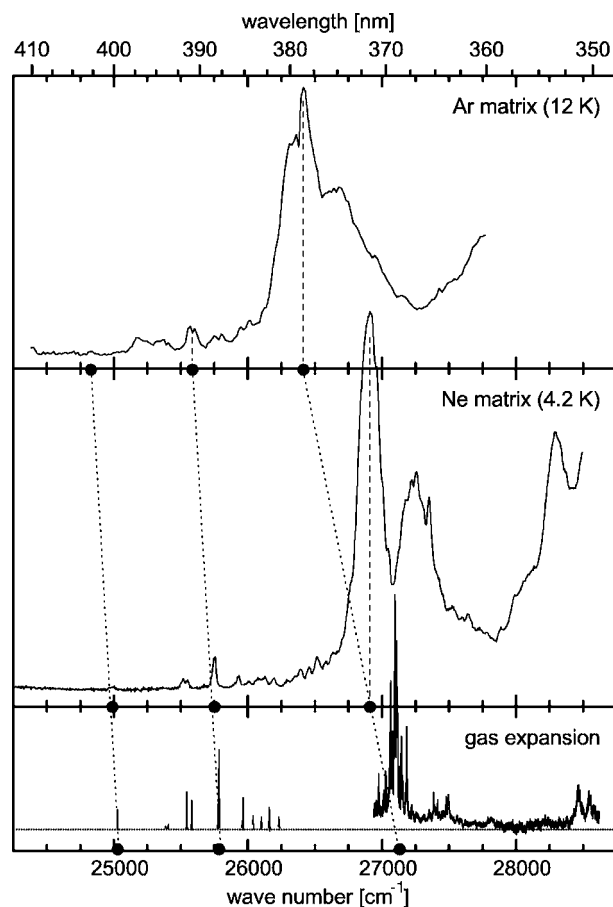


FIG. 5. Absorption spectra covering the region of the $S_2(^1B_1) \leftarrow S_0(^1A_1)$ and $S_1(^1A_1) \leftarrow S_0(^1A_1)$ transitions of BghiP observed in a supersonic gas expansion (bottom), in a neon matrix (middle), and in an argon matrix (top). In the gas jet spectrum, bands of $S_1 \leftarrow S_0$ are shown without their background. The $S_2 \leftarrow S_0$ spectrum (above 27 000 cm⁻¹) is from Ref. 5. Dashed lines indicate the positions of some notable features. The dotted lines are guides to the eye showing how the positions of particular features vary according to the environment of the molecule. Wavelengths are given for vacuum.

CRLAS measurements. Moreover, it is possible to compare our spectrum with the absorption spectrum of perylene embedded in an argon matrix.³⁷ The same bands, previously used to verify the absence of perylene in the neon matrix spectrum, would appear in solid argon at 404.7, 408.1, and 410.0 nm. Since they are not clearly discernible in the present spectrum, our conclusion is that the observed bands are not related to perylene.

While the bands of the $S_1 \leftarrow S_0$ transition observed in a neon matrix were easily identified with the help of the jet-cooled spectrum, such a procedure is not straightforward for the argon matrix data. All features are even broader than observed in the neon matrix and show a double peak structure. However, it is known from emission spectroscopy that the origin band position is at 24 828 cm⁻¹ in vacuum or 402.66 nm in air.²¹ As a consequence, the strongest feature at 25 601 cm⁻¹ corresponds with the strongest features in the neon matrix and supersonic jet spectra.

We have already noted that the energy separation between S_1 and S_2 is smaller in the neon matrix spectrum (1921 cm⁻¹) than in the jet-cooled spectrum (2105 cm⁻¹). In the argon matrix spectrum, this separation is with 1585 cm⁻¹ even smaller.

TABLE III. Comparison between electronic transition energies calculated by ZINDO and TD-DFT techniques and observed values. Numbers in parentheses are calculated oscillator strengths.

S_j, S_i	Calculated $S_j \leftarrow S_i$						Observed $S_j \leftarrow S_i$ (0-0)
	ZINDO ^a		ZINDO ^b		TD-DFT ^c		
	(cm ⁻¹)	(0.4748)	(cm ⁻¹)	(0.3978)	(cm ⁻¹)	(0.27)	
S_2, S_0	28 857	(0.4748)	26 836	(0.3978)	27 401	(0.27)	27 132 ^c
S_1, S_0	26 585	(0.0020)	26 421	(0.0028)	27 217	(0.000 27)	25 027 ^b
S_2, S_1	2272		412		184		2105

^aReference 30.^bThis work.^cReference 5.

IV. DISCUSSION

In order to devise possible candidates for DIB carriers to be studied in the laboratory, one would like to be able to calculate electronic transition energies and oscillator strengths with reasonable accuracy. Results of such calculations for BghiP are presented in Table III, where the electronic transition energies are compared with the measured origin band positions of $S_2 \leftarrow S_0$ and $S_1 \leftarrow S_0$. The calculated electronic transition energies do not include the differences between the zero point energies in the ground and excited states, but they are not expected to play a decisive role in this comparison if we assume that the vibrational modes in either state are not significantly different. The most favorable comparison is obtained when the semiempirical ZINDO technique is applied to the experimentally determined structure of BghiP.⁵⁰ Only the energies seem to be overestimated by approximately 6.3%. On the other hand, the DFT-based calculation,⁵ while yielding a good value for the $S_2 \leftarrow S_0$ transition energy, has failed to deliver an acceptable estimation of the $S_1 \leftarrow S_0$ transition energy. As a consequence, the energy difference between S_1 and S_2 is underestimated by one order of magnitude.

The cause for the better results of the ZINDO calculation is well known. Semiempirical models make use of parameters determined by experiments whereas the *ab initio* and DFT models are based on first principles. This makes the use of the latter models far more complex, and the approximations with which they are handled greatly influence the results. But *ab initio* and DFT models have the advantage over semiempirical models that they do not require any input from the experiment. For instance, the results of ZINDO calculations are rather sensitive to bond lengths and angles. The favorable results of Palewska and Chojnacki³⁰ are based on an experimentally determined structure of BghiP. Using the GAUSSIAN 03 package,³⁸ we have applied the same technique to a theoretical ground state structure determined by a tight optimization at the PM3 (Ref. 39) level, and the result is very different from what has been obtained by Palewska and Chojnacki as can be seen in Table III. Therefore, irrespective of the calculation technique used, predicting the energy of electronic states in order to identify astrophysically interesting candidates for spectroscopic investigations remains a challenge.

Examination of the vibronic intensity pattern shows that the origin band which corresponds to a transition to a totally

symmetric state is weaker than several vibronic bands relating to the excitation of nontotally symmetric b_1 modes. The weakness of the origin band is consistent with the low theoretical oscillator strength of the $S_1 \leftarrow S_0$ transition (see Table III). It is noted that, even though they are allowed, transitions to excited totally symmetric a_1 modes are not observed. This is interpreted as being due to the associated Franck-Condon factors which are expected to be much smaller than for the origin band and to negligible vibronic coupling with other states. As a consequence, the $(a_1)_0^1$ bands are too weak to be detected under the conditions of our experiment. What makes bands related to b_1 modes so strong is intensity borrowing through vibronic interaction between S_1 and S_2 , a phenomenon that has been treated by Geldof *et al.* with pyrene as an example.⁴⁰

The vibronic intensity pattern observed in the present jet-cooled absorption spectrum is a mirror image of one of the two perpendicular components of the polarized fluorescence spectrum observed with benzo[*g,h,i*]perylene in a triphenylene matrix at 4.2 K.⁴¹ This component corresponds to emissions towards b_1 vibrational levels of the electronic ground state. The good agreement supports the assumption made above that the vibrational modes in either states are not significantly different. But, while bands involving excited a_1 modes are not visible in the jet-cooled absorption spectrum, emission bands towards a_1 vibrational levels of the electronic ground state were clearly observed.⁴¹ This is explained as follows. First, emission spectroscopy is more sensitive making it possible to observe the $(a_1)_0^0$ emission bands of BghiP. Second, the intensity-borrowing phenomenon is not symmetric with respect to emission and absorption intensities,⁴⁰ with the consequence that the $(b_1)_0^0$ absorption bands are much stronger than the $(a_1)_0^0$ bands, while $(b_1)_1^0$ and $(a_1)_1^0$ emission bands are similar in intensity.

It has already been mentioned that the spectrum in the region of the $S_2(^1B_1) \leftarrow S_0(^1A_1)$ origin was investigated by Tan and Salama.⁵ The main bands in the intermediate level structure arising from the vibronic interaction of S_1 and S_2 showed widths on the order of 7 cm⁻¹, while a value of 3 cm⁻¹ was expected for the rotational temperature of about 50–60 K. The broader bandwidth in the intermediate level structure is attributed to the internal-conversion process via the vibronic interaction between S_1 and S_2 and the intersystem crossing to nearby triplet states.⁵ In contrast, the bandwidths observed in the present study of the $S_1 \leftarrow S_0$ system

are around 2.7 cm^{-1} for a rotational temperature of 40 K. We conclude that the mechanisms which cause the broadening of the bands near the origin of the $S_2 \leftarrow S_0$ transition are not effective in the range we have investigated.

Another result is important in connection with the study of the $S_2(^1B_1) \leftarrow S_0(^1A_1)$ transition. The best result to simulate the band pattern in the observed intermediate level structure suggested that the position of the origin band of $S_1 \leftarrow S_0$ was around $25\,795 \text{ cm}^{-1}$.⁵ The procedure required to define a resonance range which was chosen to spread 500 cm^{-1} on either side of the $S_2 \leftarrow S_0$ origin. It was also necessary to fix the energy separation between the $S_1(0)$ and $S_2(0)$ vibronic states in order to determine which vibrational states of S_1 fell into this resonance range. These states were considered to interact with $S_2(0)$. In the calculation, Tan and Salama took a too small energy separation of 1310 cm^{-1} (note that the actual energy separation determined by the present study is 2105 cm^{-1}). This value was slightly increased to 1337 cm^{-1} , in order to obtain a better agreement between the simulated and observed intermediate level structure, which finally led to the suggested position of $25\,795 \text{ cm}^{-1}$ for the $S_1 \leftarrow S_0$ origin. But the separation of 1337 cm^{-1} is still much smaller than the experimental value determined in the present study. Therefore, the vibrational states of S_1 falling into the resonance range would be different, leading to a new assignment of the intermediate level structure observed in the $S_2 \leftarrow S_0$ spectrum.

Since we have determined that the $S_1 \leftarrow S_0$ origin band is at $25\,027.1 \text{ cm}^{-1}$, the bands corresponding to the fundamental excitation of the CH-stretching modes, which are of the a_1 and b_1 species, are expected in the region near $28\,100 \text{ cm}^{-1}$. This region was covered in the investigation of the $S_2 \leftarrow S_0$ transition by Tan and Salama,⁵ but it did not reveal any band there, indicating that the CH-stretching bands are very weak, independent of the fact whether the relevant modes are of a_1 or b_1 species.

The redshifts observed for the positions of the $S_1 \leftarrow S_0$ and $S_2 \leftarrow S_0$ transitions in neon and argon matrices relative to the gas phase positions yield information on the permanent electric dipole moment and polarizability of the molecule in the different electronic states. In the case of polycyclic aromatic hydrocarbons in rare gas matrices, it is actually expected that the main contribution is caused by the change of polarizability during the transition since most PAHs are either nonpolar or very weakly polar molecules. This change causes a variation of the dispersion energy of the system represented by the molecule and the surrounding matrix. Extracting values for the variations of the components of the polarizability tensor during transition cannot be done in a straightforward way. It is necessary to know the relative positions of the solvent atoms and of the solute molecule for that purpose.

Nevertheless, the different values observed for the energy separation between states S_1 and S_2 under the different environments yield some rough quantitative information on the polarizability of these states. In a basic model, the dispersion interaction energy between a molecule and the surrounding medium is considered to be proportional to both the mean static dipole polarizability of the molecule and the po-

larizability of the medium. The matrix-induced redshift of $S_n \leftarrow S_0$ ($n=1,2$) is larger in argon than in neon because of the larger polarizability of argon. And for a given matrix material, the redshift is larger for $S_2 \leftarrow S_0$ than for $S_1 \leftarrow S_0$ since the mean static dipole polarizability of benzo[*g,h,i*]perylene is higher in its S_2 state than in its S_1 state. From the comparison of the jet-cooled and argon matrix spectra, one can deduce that the increase of the dispersion interaction energy is roughly 3.6 times larger for $S_2 \leftarrow S_0$ than for $S_1 \leftarrow S_0$. The mean polarizability is assumed to vary in the same proportion. This factor is similar to those that can be determined for phenanthrene and 1,2-5,6-dibenzanthracene, the mean polarizabilities of which were investigated by solvatochromy.⁴² The respective values are 3.4 and 3.1. Moreover, the same factor is 4.1 in the case of pyrene, as deduced from the spectroscopic investigation of this molecule embedded in a polymethylmetacrylate film.⁴³ Accordingly, such a simple model yields values between 3 and 6 for the ratio of the argon to neon environment polarizabilities, which is consistent with the ratio of argon to neon atomic polarizabilities.

The perylene bands in Fig. 1(a), where the sample was heated to $235 \text{ }^\circ\text{C}$, have almost the same intensities as those in Fig. 1(b) where the temperature was only $156 \text{ }^\circ\text{C}$ (the latter being 30% stronger). Therefore, the density of perylene in the jet was similar in both experiments. Since the vapor pressure of perylene at $235 \text{ }^\circ\text{C}$ is considerably higher than at $156 \text{ }^\circ\text{C}$, with 73 Pa against 0.20 Pa,⁴⁴ this means that, in the experiments with BghiP, the perylene molecules were probably trapped in the BghiP crystals and evaporated at the same rate as the BghiP molecules. Therefore, having determined by HPLC that the solid BghiP sample contained 1% of perylene, the density of perylene in the jet should be approximately 1% of that of BghiP. This is consistent with the fact that, if a species in a binary mixture has a very low concentration, its vapor pressure is expected to be very close to that of the main species, in analogy to the application of Raoult's law to ideal liquid binary mixtures. As a consequence, given that the observed perylene bands exhibit intensities comparable to those of the BghiP bands, one may conclude that their absorption cross sections are two orders of magnitude larger than those of the BghiP bands.

Finally, the vapor pressure of benzo[*g,h,i*]perylene at $235 \text{ }^\circ\text{C}$ can be estimated. If the density of perylene in the source at $235 \text{ }^\circ\text{C}$ was equivalent to a partial pressure of 0.20 Pa and the density of perylene was 1% of that of BghiP, one can deduce that the vapor pressure of BghiP was about 20 Pa in the source. This value is reasonable given that the vapor pressures of perylene and coronene at $235 \text{ }^\circ\text{C}$ are 73 and 1.2 Pa, respectively.⁴⁴

V. CONCLUSIONS

The position of the origin band for the $S_1(^1A_1) \leftarrow S_0(^1A_1)$ transition of benzo[*g,h,i*]perylene ($\text{C}_{22}\text{H}_{12}$) has been measured by absorption spectroscopy in a supersonic jet at $25\,027.1 \pm 0.2 \text{ cm}^{-1}$. This assignment is supported by the measured rotational band profile which is a *B* type. It is also supported by the observation of several other bands,

whose positions have been measured too. The fundamental vibrational frequencies derived from these measurements are consistent with published calculated frequencies. Except for the origin band, all bands for which a rotational contour could be measured involve the fundamental excitation of modes with b_1 symmetry since they all exhibit an A -type profile. Concerning the remaining bands, they are also assigned to excitations of b_1 modes, though sometimes tentatively. None of the bands could be definitely related to excited a_1 modes even though such transitions are allowed. This indicates that they were too weak to be detected under the experimental conditions while the intensity of bands related to b_1 modes is enhanced by intensity borrowing through vibronic interaction between S_1 and S_2 . This is the simplest explanation for our observations. The involvement of higher electronic states should be considered if more detailed experimental studies are available.

The $S_1 \leftarrow S_0$ transition of benzo[g,h,i]perylene has been investigated by matrix isolation spectroscopy in neon at 4.2 K as well as in argon at 12 K. The comparison of the matrix spectra with the jet-cooled spectrum supports the previous analysis.

Examination of the energy shifts for the $S_1 \leftarrow S_0$ and $S_2 \leftarrow S_0$ transitions observed in the gas phase and in the two rare gas matrices shows that the variation of dispersion energy in $S_2 \leftarrow S_0$ is by a factor of 3.6 larger than in $S_1 \leftarrow S_0$, meaning that the polarizability of BghiP is higher in the S_2 state than in the S_1 state.

As far as the interpretation of the diffuse interstellar bands is concerned, the comparison of the BghiP spectrum with astronomical databases does not lead to any positive identification. This can be due to the fact that the first strong transition of BghiP, $S_2 \leftarrow S_0$, near 369 nm is out of the ranges covered by current DIB surveys, which extend between 400 and 800 nm. Yet, an interesting point is that the band contour analysis in $S_1 \leftarrow S_0$ has yielded a bandwidth of 2.7 cm^{-1} associated with a rotational temperature close to 40 K. This supports the assumption that neutral polycyclic aromatic hydrocarbons are better candidates as DIB carriers than their cations which exhibit bandwidths of the order of $20\text{--}30 \text{ cm}^{-1}$ in relation with their short lifetime.⁴ To date, only a few neutral PAHs, presenting an $S_1 \leftarrow S_0$ transition at wavelengths longer than 400 nm, have been studied in supersonic gas expansions. Firmer conclusions on a potential correlation between neutral PAH molecules and DIBs must await a larger set of laboratory data.

ACKNOWLEDGMENTS

This work was carried out within a cooperation between the Max-Planck-Institut für Astronomie and the Friedrich-Schiller-Universität Jena. The support of the Deutsche Forschungsgemeinschaft is gratefully acknowledged. The authors are grateful to Professor I. Y. Chan for providing unpublished spectra of coronene containing traces of benzo[g,h,i]perylene. The authors wish to thank H. Mutschke for making his setup for matrix isolation spectroscopy available to them and C. Jäger for the HPLC analysis. One of the authors (F.S.) acknowledges the support of the APRA

program of the National Aeronautics and Space Administration (NASA). This research was performed while another author (X.T.) held a NASA Postdoctoral Program (NPP) Fellowship at NASA Ames Research Center.

- ¹F. Salama, G. A. Galazutdinov, J. Krelowski, L. J. Allamandola, and F. A. Musaev, *Astrophys. J.* **526**, 265 (1999).
- ²G. Rouillé, S. Krasnokutski, F. Huisken, T. Henning, O. Sukhorukov, and A. Staicu, *J. Chem. Phys.* **120**, 6028 (2004).
- ³A. Staicu, G. Rouillé, O. Sukhorukov, T. Henning, and F. Huisken, *Mol. Phys.* **102**, 1777 (2004).
- ⁴X. Tan and F. Salama, *J. Chem. Phys.* **122**, 084318 (2005).
- ⁵X. Tan and F. Salama, *J. Chem. Phys.* **123**, 014312 (2005).
- ⁶L. Biennier, F. Salama, L. J. Allamandola, and J. J. Scherer, *J. Chem. Phys.* **118**, 7863 (2003).
- ⁷L. Biennier, F. Salama, M. Gupta, and A. O'Keefe, *Chem. Phys. Lett.* **387**, 287 (2004).
- ⁸O. Sukhorukov, A. Staicu, E. Diegel, G. Rouillé, T. Henning, and F. Huisken, *Chem. Phys. Lett.* **386**, 259 (2004).
- ⁹X. Tan and F. Salama, *Chem. Phys. Lett.* **422**, 518 (2006).
- ¹⁰E. V. Shpolskii, *Sov. Phys. Usp.* **2**, 51 (1959).
- ¹¹J. P. Toennies and A. F. Vilesov, *Angew. Chem., Int. Ed.* **43**, 2622 (2004).
- ¹²J. Aihara, K. Ohno, and H. Inokuchi, *Bull. Chem. Soc. Jpn.* **43**, 2435 (1970).
- ¹³E. Clar, *Ber. Dtsch. Chem. Ges. B* **65**, 846 (1932).
- ¹⁴W. R. Dawson and J. L. Kropp, *J. Phys. Chem.* **73**, 1752 (1969).
- ¹⁵T. Kajiwara, I. Shirovani, H. Inokuchi, and S. Iwashima, *J. Mol. Spectrosc.* **29**, 454 (1969).
- ¹⁶J. Langelaar, J. W. van Beek, J. D. W. van Voorst, and D. Lavalette, *Chem. Phys. Lett.* **6**, 460 (1970).
- ¹⁷J. L. Richards and S. A. Rice, *Chem. Phys. Lett.* **9**, 444 (1971).
- ¹⁸K. A. Hodgkinson and I. H. Munro, *J. Mol. Spectrosc.* **48**, 57 (1973).
- ¹⁹J. B. Birks, C. E. Easterly, and L. G. Christophorou, *J. Chem. Phys.* **66**, 4231 (1977).
- ²⁰N. Nijegorodov, R. Mabbs, and W. S. Downey, *Spectrochim. Acta, Part A* **57**, 2673 (2001).
- ²¹X. Chillier, P. Boulet, H. Chermette, F. Salama, and J. Weber, *J. Chem. Phys.* **115**, 1769 (2001).
- ²²A. Nakajima, *Bull. Chem. Soc. Jpn.* **45**, 1687 (1972).
- ²³L. A. Nakhimovsky, M. Lamotte, and J. Jousot-Dubien, *Handbook of Low Temperature Electronic Spectra of Polycyclic Aromatic Hydrocarbons*, Physical Sciences Data, Vol. 40 (Elsevier, Amsterdam, 1989).
- ²⁴R. S. Mulliken, *J. Chem. Phys.* **23**, 1997 (1955).
- ²⁵P. M. Saari and T. B. Tamm, *Opt. Spektrosk.* **40**, 691 (1976) [*Opt. Spectrosc.* **40**, 395 (1976)].
- ²⁶G. Bermudez and I. Y. Chan, *J. Phys. Chem.* **90**, 5029 (1986).
- ²⁷I. Renge, *Chem. Phys.* **295**, 255 (2003).
- ²⁸R. L. Hummel and K. Ruedenberg, *J. Phys. Chem.* **66**, 2334 (1962).
- ²⁹J. Marañón, O. M. Sorarrain, and A. L. Capparelli, *Z. Phys. Chem. (Leipzig)* **254**, 73 (1973).
- ³⁰K. Palewska and H. Chojnacki, *J. Mol. Struct.* **611**, 23 (2002).
- ³¹J. Ridley and M. Zerner, *Theor. Chim. Acta* **32**, 111 (1973); M. C. Zerner, G. H. Loew, R. F. Kirchner, and U. T. Mueller-Westerhoff, *J. Am. Chem. Soc.* **102**, 589 (1980); M. C. Zerner, in *Reviews in Computational Chemistry II*, edited by K. B. Libkowitz and D. B. Boyd (VCS, NY, 1991), pp. 313–366.
- ³²NIST Atomic Spectra Database (<http://physics.nist.gov/PhysRefData/ASD/index.html>).
- ³³D. Romanini and K. K. Lehmann, *J. Chem. Phys.* **99**, 6287 (1993).
- ³⁴S. Leutwyler, *J. Chem. Phys.* **81**, 5480 (1984).
- ³⁵See EPAPS Document No. E-JCPSA6-126-010717 for tables and comments on the positions and assignments of perylene and perylene•Ar_n ($n=1,2$) absorption bands in the 24 059–26 182 cm^{-1} range. This document can be reached via a direct link in the online article's HTML reference section or via the EPAPS homepage (<http://www.aip.org/pubservs/epaps.html>).
- ³⁶V. L. Stakhursky and T. Miller, Proceedings of the 56th Molecular Spectroscopy Symposium, 2001 (unpublished).
- ³⁷C. Joblin, F. Salama, and L. Allamandola, *J. Chem. Phys.* **110**, 7287 (1999).
- ³⁸M. J. Frisch, G. W. Trucks, H. B. Schlegel *et al.*, GAUSSIAN 03, Revision C.02, Gaussian, Inc., Pittsburgh PA, 2003.

³⁹J. J. P. Stewart, J. Comput. Chem. **10**, 209 (1989); **10**, 221 (1989).

⁴⁰P. A. Geldof, R. P. H. Rettschnick, and G. J. Hoytink, Chem. Phys. Lett. **10**, 549 (1971).

⁴¹K. Ohno and H. Inokuchi, Chem. Phys. Lett. **33**, 585 (1975).

⁴²I. Renge, Chem. Phys. **167**, 173 (1992).

⁴³S. Umeuchi, Y. Nishimura, I. Yamazaki, H. Murakami, M. Yamashita, and N. Ohta, Thin Solid Films **311**, 239 (1997).

⁴⁴V. Oja and E. M. Suuberg, J. Chem. Eng. Data **43**, 486 (1998).